Steel and Composite Structures, *Vol. 37, No. 3* (*2020*) *259-272*
DOI: https://doi.org/10.12989/scs.2020.37.3.259

Steel hysteretic column dampers for seismic retrofit of soft-first-story structures

Mohammad Mahdi Javidan[a] and Jinkoo Kim*

Department of Civil & Architectural Engineering, Sungkyunkwan University, Suwon, Republic of Korea

(*Received December 5, 2019, Revised October 1, 2020, Accepted October 13, 2020*)

Abstract. In this study a new hysteretic damper for seismic retrofit of soft-first story structures is proposed and its seismic retrofit effect is evaluated. The damper consists of one steel column member and two flexural fuses at both ends made of steel plates with reduced section, which can be placed right beside existing columns in order to minimize interference with passengers and automobiles in the installed bays. The relative displacement between the stories forms flexural plastic hinges at the fuses and dissipate seismic energy. The theoretical formulation and the design procedure based on plastic analysis is provided for the proposed damper, and the results are compared with a detailed finite-element (FE) model. In order to apply the damper in structural analysis, a macromodel of the damper is also developed and calibrated by the derived theoretical formulas. The results are compared with the detailed FE analysis, and the efficiency of the damper is further validated by the seismic retrofit of a case study structure and assessing its seismic performance before and after the retrofit. The results show that the proposed hysteretic damper can be used effectively in reducing damage to soft-first story structures.

Keywords: seismic retrofit; soft story; hysteretic dampers; seismic performance; energy dissipation device

1. Introduction

Currently many low-rise residential buildings in Korea are built using reinforced concrete (RC) load-bearing wall systems supported by columns in the first story to provide open space for parking lot. Many of these structures have eccentrically located core shear walls surrounding the staircase. As a result, these structures have seismic vulnerability of both the vertical (soft-first story) and the plan-wise irregularities. A common example of these structures is shown in Fig. 1(a). A lot of these soft first-story structures were heavily damaged during the 2017 Pohang earthquake with the magnitudes of 5.4 M_w, as depicted in Fig. 1(b), where shear failure of the first story columns was the main failure mechanism. It was also observed that in many cases the shear failure of columns was aggravated due to the insufficient transverse reinforcement. Currently, there is a growing need in Korea to reinforce these structures using retrofit schemes which are inexpensive and do not block the open space in the first story.

Seismic performance of structures with irregularities have been investigated in several studies, and various retrofit schemes have been proposed. Sahoo and Rai (2013) proposed a retrofit technique using chevron braces at the ground story connected to the structure with aluminum shear links to dissipate the energy. Shin *et al*. (2014) analyzed a two-dimensional frame of a soft-first story structure under successive earthquakes, with and without retrofit after the main shock. They chose buckling-restrained braces for this purpose and conducted a systematic fragility analysis. They showed that the behavior of the structure under the aftershock is significantly affected by the severity of the main shock and the effectiveness of the retrofit depends also on the damage state after the first earthquake. Kim and Jeong (2016) applied slit dampers to story-wise and plan-wise irregular structures. They showed that larger drift demands exist at the flexible side in a plan layout and the retrofit should be done so that the torsional irregularity is reduced.

In a recent study, Dang-vu *et al*. (2019) evaluated the effects of shear-axial force interactions on a case study structure severely damaged by an earthquake. They concluded that considering the shear effects can significantly impact the seismic response of the studied structure.

There are wide variety of different seismic retrofit strategies and energy dissipation devices, including damped-cable system (Naeem and Kim 2018a, b), seismic isolation (Öncü-Davas and Alhan 2019a, b), viscoelastic dampers (Kim and Bang 2003, Xu 2009, Xu *et al*. 2016, 2020, Javidan and Kim 2020), friction dampers (Mualla and Belev 2002, Kim and Kim 2017, Yousef-beik *et al*. 2020), etc. Owing to a stable hysteretic behavior and easy manufacturing, hysteretic dampers are widely applied in different schemes and forms. Whittaker *et al*. (1991) evaluated steel plate added damping and stiffness (ADAS) system which dissipates energy using out-of-plane bending of steel plates, and Tsai *et al*. (1998) investigated the one with triangular plates (TADAS). Chan and Albermani (2008) developed a weld free and an easy to manufacture energy dissipation device by cutting a series of slits through the web of a short length wide-flange section. The proposed

*Corresponding author, Professor
E-mail: jkim12@skku.edu
[a]Research assistant

ISSN: 1229-9367 (Print), 1598-6233 (Online)

(a)

(b)

Fig. 1 Example of soft-first-story structures in Korea: (a) overall configuration and (b) common failure mechanism observed in the 2017 Pohang earthquake (Photographs taken by the corresponding author)

device was tested under cyclic loads and it showed a very stable and ductile behavior. The seismic performance of steel slit dampers was further investigated by Kim *et al.* (2017), Lee and Kim (2017), and Nour Eldin *et al*. (2018). Naeem and Kim (2019) developed a multi-slit damper which has a low yield strength at small drift and higher strength at large drift.

Buckling-restrained braces (BRBs, also known as unbonded braces) are sort of metallic dampers displaying a balanced hysteretic behavior by axial yielding under reversed cyclic tension and compression forces during major earthquakes. The seismic performance of the buckling restrained braces has been investigated by many researchers (Kim and Choi 2004, Kim *et al*. 2009, Park *et al*. 2012, Mohammadi *et al.* 2018, Mohammadi *et al.* 2020), and they are widely applied in Japan and in the USA as ductile energy dissipating braces. When compared to other alternative seismic energy dissipation systems, BRBs have advantages such as easy replacement following an earthquake, easy fabrication and construction with relatively low cost, simple end connection details, etc.

Many conventional seismic retrofit schemes tend to block the bays in the first story. To solve this problem, Agha Beigi *et al*. (2014) proposed a gapped-inclined brace installed beside columns to reduce the P-Delta effects and share the lateral loads after reaching a predefined interstory drift. They observed that the proposed retrofit strategy can increase the post yield stiffness while not affecting the lateral resistance significantly. Javidan and Kim (2019) developed a retrofit scheme using rotational friction dampers at the beam-column joint, and evaluated its efficiency by carrying out an experimental cyclic loading test.

In the present research, a new hysteretic energy dissipation device for seismic retrofit of structures is proposed and its applicability is evaluated through theoretical formulation, detailed finite-element (FE) analysis, and application in seismic retrofit of a case study structure. The device is a steel column member with a hysteretic damper at both ends, and is installed vertically between stories. The proposed damper can be installed beside existing columns to retrofit the structure, and can be easily applied not only to soft-first story structures but also to other types of structures in order to provide seismic energy dissipation capacity while the required architectural space is secured. Details of the proposed scheme are elaborated, and the theoretical formulation based on elastoplastic analysis is derived for both analysis and design. A design procedure for the damper to meet a target drift ratio is suggested, and the procedure is demonstrated for the maximum considered earthquake (MCE) level. The cyclic behavior of the designed damper is evaluated through an FE analysis. For structural analysis, a macromodel for the damping device is developed using elastic elements and nonlinear rotational springs calibrated by the derived theoretical formulation, and the results are compared with the time-consuming detailed FE analysis. The efficiency of the proposed retrofit scheme is further verified by applying the retrofit strategy to a case study structure, and comparing the seismic performance with the results before the retrofit in terms of maximum and average interstory drift ratio, residual displacement, and energy dissipation of the dampers.

2. Proposed hysteretic damper

2.1 Description

The aim of this research is to develop a damper for seismic retrofit of soft-first story structures which can be located beside the existing columns on the first story, in order not to block the access to the parking space. In these structures, the input seismic energy is mostly dissipated by the flexural plastic hinges formed at the end of columns. Inspired by this phenomenon, a new type of energy dissipation device composed of a steel column with designated hysteretic fuses at the ends is developed to be installed right beside the current RC columns. The proposed scheme is demonstrated in Fig. 2.

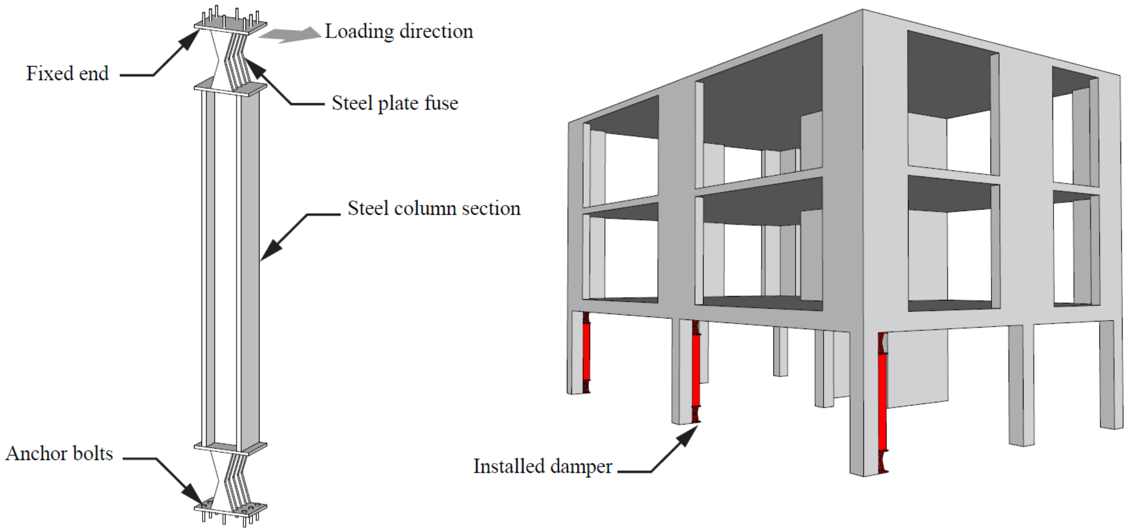

(a) (b)

Fig. 2 Proposed retrofit scheme: (a) configuration of the damper and (b) installation scheme.

To this end, a H-shaped steel section is chosen for the column member which has an elastic modulus large enough to maintain small elastic deformation before plastic hinge formation in the fuses. Each fuse is composed of several steel plates with reduced mid-height width as the designated yield point. By changing the mid-height width of the fuse, the yield strength of the damper can be controlled. The fuse yields under flexural action which is imposed by the interstory drift and the following rotation at both ends of the steel column. Since the steel plates yield in-plane, this type of fuse can provide higher capacity compared to conventional ADAS (Whittaker *et al.* 1991) and TADAS (Tsai *et al.* 1998) dampers which yield out-of-plane (Lee *et al.* 2017). In addition, ADAS and TADAS are usually applied to the structure using chevron braces which block the whole bay.

Compared with the conventional steel hysteretic devices, the proposed column damper has advantage in providing additional stiffness and energy dissipation capacity while only small space is required for installation.

2.2 Theoretical formulation

In this section the analysis model of the column damper is derived using the plastic analysis. As the fuses are located at the ends of the column where bending moment is the maximum, the yield strength of the damper can be calculated assuming that the flexural plastic hinges are formed at the fuse locations. The free-body diagram of the damper at the yield state is shown in Fig. 3. Based on the free-body diagram and the virtual work equation, the capacity of the damper at the yield displacement Δ can be determined as

$$F\Delta = 2M_p\theta \tag{1}$$

where F is yield force of the damper, Δ is the yield displacement equal to the inter-story drift, M_p is plastic moment of the fuse section, and θ is the rotation of the fuse equal to Δ/l. The full moment capacity of the fuse M_p can be calculated by

$$M_p = n\frac{tw_1^2}{4}\sigma_y \tag{2}$$

where n is the number of steel plates in the fuse, t and w_1 are respectively the thickness and width of the steel plate at the reduced section, and σ_y is the yield strength of the steel plates. By substituting those parameters in Eq. 1, the yield capacity of the damper is obtained as

$$F = n\frac{tw_1^2}{2l}\sigma_y \tag{3}$$

It can be observed that increasing the width of the reduced section can increase the capacity of the damper to the power of two, and that the thickness and number of steel plates are directly proportional to the yield strength.

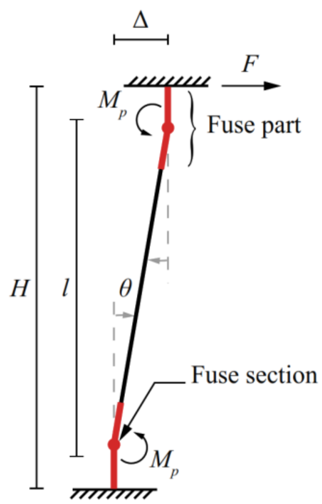

Fig. 3 Analysis model of the proposed damper

The elastic deformation of the damper Δ prior to the yield mechanism can be determined by considering deformations of the fuses and the steel column in series. This can be determined by calculating the slope θ and then finding the deflection with integration all along the length of the damper. The bending moment is a piecewise function which is equal to M_p from the fixed end to the fuse section and increases linearly from there to the other fuse section and over the column. The fuse part of the damper consists of two tapered sections which needs to be considered in the integration. The slope can be calculated as follows

$$\theta(x) = \int_0^x \frac{M(x)dx}{EI(x)} \tag{4}$$

where E is the elastic modulus of steel, $M(x)$ is the bending moment function, and $I(x)$ is the moment of inertia. For this problem, bending moment $M(x)$ in the numerator is a linearly piecewise function, and the moment of inertia $I(x)$ in the denominator is a cubic piecewise function. The slope determined from this equation needs to be integrated once again to obtain the deflection, which makes it hard to derive and calculate. As mentioned earlier, the bending moment from the fuse section to the fixed end is constant. Since the other half of the reduced section has also a relatively short length, it can be assumed that the bending moment is constant all over the fuse part to simplify the calculation. The rotation along the fuse part is a piecewise function because of the changing moment of inertia. The moment of inertia is determined by

$$I = \begin{cases} \dfrac{n}{12}t(w_2 - \dfrac{w_2 - w_1}{\left(\dfrac{H-l}{2}\right)}x)^3 & 0 \le x \le \dfrac{H-l}{2} \\ \dfrac{n}{12}t(w_1 - \dfrac{w_1 - w_2}{\left(\dfrac{H-l}{2}\right)}x)^3 & \dfrac{H-l}{2} \le x \le H-l \end{cases} \tag{5}$$

where w_2 is the larger width of the plate tapered to the width of w_1 at the fuse section. By considering a constant bending moment $M(x)$ equal to M_p and substituting in Eq. (5), the piecewise rotation function $\theta\ (x)$ is determined as

$$\theta = \begin{cases} \dfrac{3M_p(H-l)}{nEt(w_2-w_1)} \times [(w_2 - \dfrac{w_2-w_1}{\left(\dfrac{H-l}{2}\right)}x)^{-2} - w_2^{-2}] \\ 0 \le x \le \dfrac{H-l}{2} \\ \dfrac{3M_p(H-l)}{nEt(w_2-w_1)} \times [2w_1^{-2} - w_2^{-2} - ((2w_1 - w_2) - \dfrac{w_1-w_2}{\left(\dfrac{H-l}{2}\right)}x)^{-2}] \\ \dfrac{H-l}{2} \le x \le H-l \end{cases} \tag{6}$$

The rotation at the end of the fuse part is obtained from Eq. (6) as

$$\theta = \frac{6M_p(H-l)(w_1+w_2)}{nEtw_1^2w_2^2} \tag{7}$$

The horizontal displacement of the fuse part Δ_1 is obtained by integrating Eq. (6) over the fuse part

$$\Delta_1 = \frac{3M_p(H-l)^2}{nEt}\frac{w_1+w_2}{w_1^2w_2^2} \tag{8}$$

The total displacement of the damper Δ can be obtained using the displacement of the fuse parts from Eq. (8), the rigid body rotation of the steel column from Eq. (7), and its deformation Δ_2 as

$$\Delta = 2\Delta_1 + (2l - H)\theta + \Delta_2 \tag{9}$$

where Δ_2 is equal to $\frac{Fl^3}{12EI_c}$, and I_c is the moment of inertia of the column section. Usually, deformations caused by the first and the last term of Eq. (9) are negligible compared to the term caused by the rotation of the fuse part. These relations are based on the fully fixed boundary condition assumption, except the lateral displacement at the top of the damper. Using the derived equations, the behavior of the damper can be properly approximated for both analysis and design.

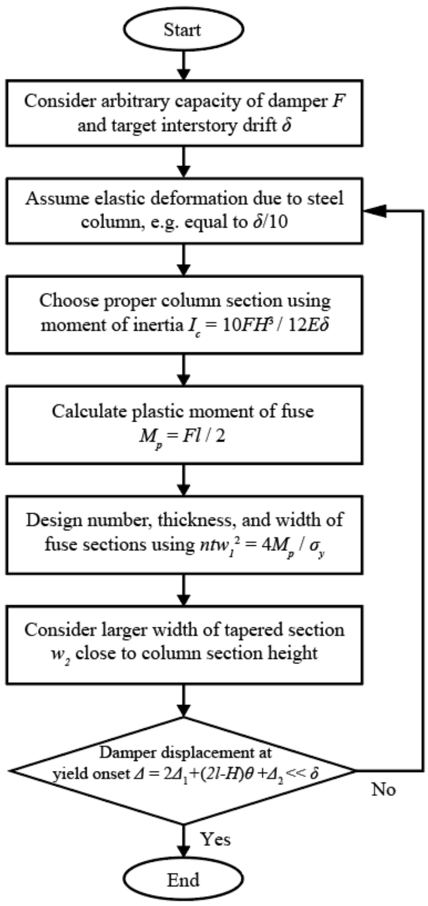

Fig. 4 Design procedure for the hysteretic-column damper

2.3 Design procedure of the damper

To design the damper with an arbitrary capacity for a considered seismic performance, limiting the elastic deformation prior to the formation of plastic hinges is the first step. As a target performance objective, it is assumed that the maximum interstory drift ratios should not exceed 1.0% and 1.5% of story height under the design basis earthquake (DBE) and the maximum considered earthquake (MCE), respectively. These limit states correspond to the life safety and the collapse prevention seismic performances, respectively. The steel column to which the hysteretic fuses are attached should be stiff enough so that all deformation is concentrated on the fuses, which enables them to be fully activated and effectively dissipate seismic energy.

The design procedure of the damper to have a given capacity is arranged as a flowchart in Fig. 4. The lateral elastic displacement in the steel column can be assumed to be less than one-tenth of the target interstory drift ratio for the design, and the remaining displacement is due to the rotation of the fuses. Having the displacement and the considered moment capacity, the moment of inertia of the column section can be obtained. Hence, a column section can be chosen based on this moment of inertia and other limitations and constraints required in the site. The number of plates in the fuse should be determined considering the dimensions of the steel column. After choosing a proper column section and the number of plates in the fuse, the plastic moment of each fuse section can be obtained. The elastic deformation of the damper can be double-checked based on the final dimensions. It is clear that the total elastic deformation prior to yield should be much smaller than the target interstory drift.

2.4 Finite element analysis

In order to evaluate the behavior of the proposed column damper, the derived formulas, and the design procedure, the damper is designed with an arbitrary yield capacity F of 100 kN and a cyclic loading test is simulated using detailed finite element (FE) analysis. The macromodel of the damper is also established and is compared with the detailed FE analysis for validation.

The damper is designed for a structure with the story height of 3m. In this case the length between the two fuse sections l is estimated to be 2.51 m. The yield strength and Young's modulus of steel are 300 MPa and 2.1×10^5 MPa, respectively. The target interstory drift is set to be 1.5% of the story height, which is 45 mm. Based on the design procedure, the elastic deformation due to the column section is limited to one-tenth of the target interstory drift, which is 4.5 mm. The section of IPB 260 is chosen for the steel column. The fuse section consists of five steel plates with a thickness of 15 mm, and the tapered width changes between 150 mm to 250 mm. The yield displacement and yield force derived using the formulas are equal to 19 mm and 101 kN, respectively.

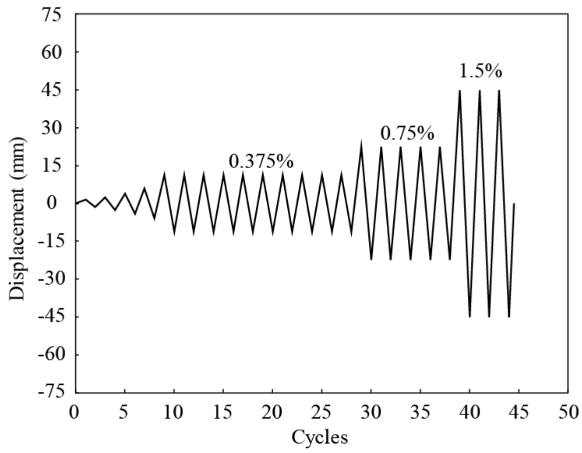

Fig. 5 Loading protocol applied to detailed FE model and macromodel

The detailed FE model of the designed damper is Workbench (2019). The accuracy of ANSYS for modeling steel hysteretic energy dissipation devices has been previously shown (Naeem and Kim 2019). The damper is modeled using 1,970 quadratic 20-node SOLID186 elements with bilinear kinematic strain hardening to consider the plasticity. Since the column section remains almost in the elastic range and the damage is concentrated at fuse part of the damper, a finer mesh is considered for the fuse sections. The fixed boundary condition is assumed for both ends of the damper. Lateral displacement is imposed on one end of the column damper following the loading protocol recommended by ASCE 41-13 (2013). The loading protocol, shown in Fig. 5, consists of ten, five, and three fully reversed cycles corresponding to 0.25, 0.5, and 1.0 times the limit state under the Maximum Considered Earthquake (MCE), respectively, which is equal to 1.5% of the story height.

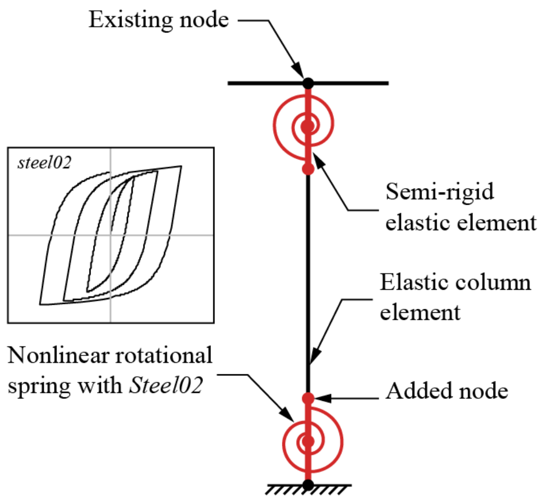

Fig. 6 Macromodel of column damper in *OpenSees*

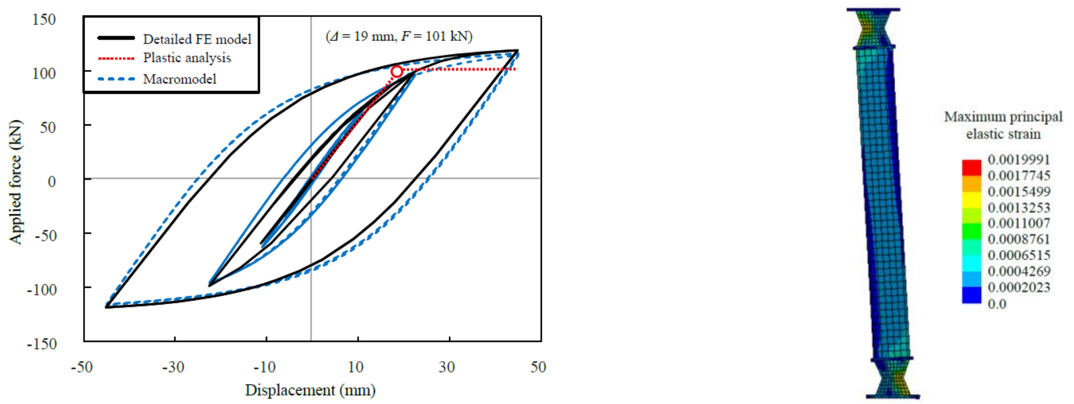

(a) (b)

Fig. 7 Hysteretic behavior of the damper: (a) Force-displacement curves obtained from FE analysis, plastic analysis, and macromodel and (b) FE mesh and the maximum principal elastic strains at 1.5% interstory drift ratio

The macromodel of the damper is developed using six added nodes, five elastic elements, and two nonlinear rotational springs in the *OpenSees* platform (Mazzoni *et al.* 2006). In order to model each fuse section, two nodes at the same location of the fuse section are added and their translational degrees of freedom (DOFs) are constrained using bar type *rigidLink*. Their rotational DOFs are constrained using nonlinear rotational spring defined using the *zeroLength* element with the *Steel02* material. To calibrate this material, the yield moment M_p is determined from Eq. (2), and the yield rotation is obtained using the corresponding lateral deformation Δ from Eq. (9). The fuse parts are modeled as semi-rigid using an elastic section with a large moment of inertia. The lateral deformation due to their elastic deformation is already considered in the provided formulas. The column is modeled using the *elasticBeamColumn* element as it is with the *Steel02* material. Since it has its elastic deformation, Δ_2 is subtracted from Eq. (9) while calibrating the rotational springs. The rotational springs are modeled using material *Steel02,* which is assumed to have a strain hardening ratio of 1%. This material follows the Giuffré-Menegotto-Pinto model (Menegotto and Pinto 1973) and contains three parameters controlling the transition from elastic to plastic branches which are calibrated based on the detailed FE model. The results of the detailed FE analysis, plastic analysis, and the macromodel are depicted and compared in Fig. 7(a). The detailed FE model of the column damper is shown in Fig. 7(b) along with the contour of the maximum principal elastic strains at the drift ratio of 1.5%.

It is observed that the behavior of the damper in the detailed FE analysis is consistent with the calculations derived using plastic analysis. The initial elastic stiffness which is calculated using the elastic analysis of the tapered fuse part and the column section is accurate. The yield force of the damper determined using the plastic analysis is also in a very good agreement, and the existing difference is due to the strain hardening and bilinear idealization. Hence, the macromodel which is also based on these formulas provides a good accuracy as expected. The advantages of macromodels and comparison with detailed models and experimental data for steel members have been done in previous studies (Usefi *et al.* 2018).

3. Application to model structure

3.1 Structural representation

To check the applicability and efficiency of the proposed damper in seismic retrofit of structures, the seismic performance of a case study structure is evaluated before and after installation of the proposed column dampers. The structure considered in this study is a 4-story RC residential building depicted in Fig. 8, which has been adopted from a real structure and was used in previous studies (Javidan and Kim 2019, Kim and Jeong 2016). The structural system of the building consists of load-bearing walls supported by columns and beams in the first story. The height of each story is 3 m and the plan layout of the structure is shown in Fig. 9. There is a core shear wall surrounding the staircase which is eccentrically located and causes plan-wise asymmetry for loads acting along the X-direction.

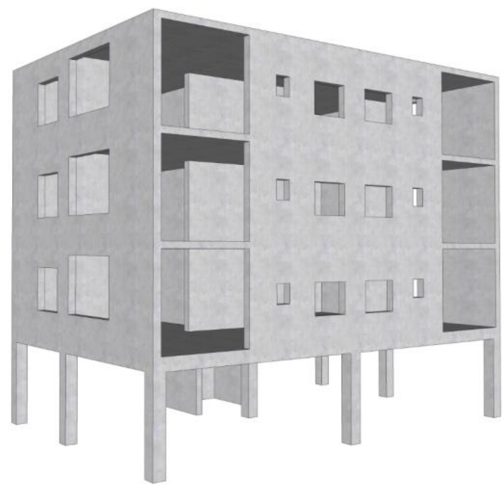

Fig. 8 Three-dimensional view of the case study structure

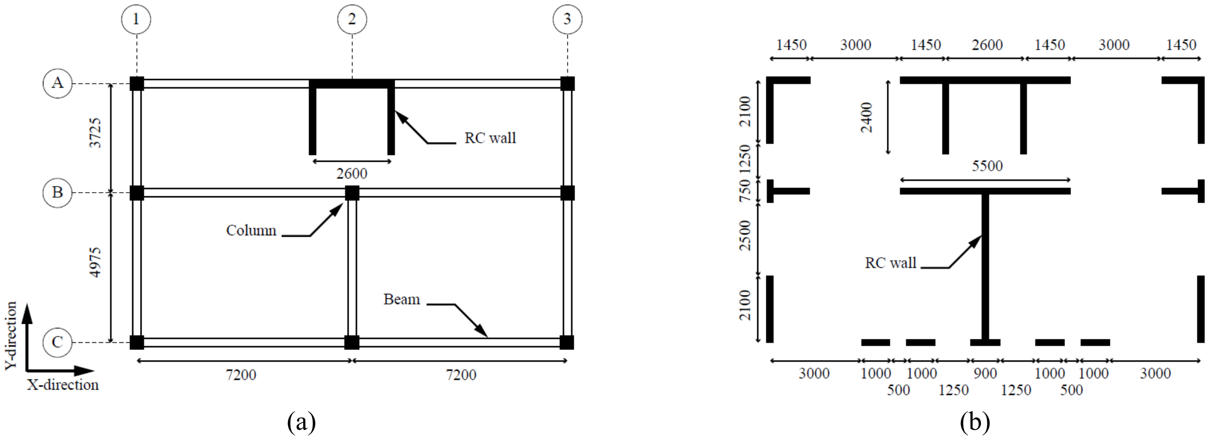

Fig. 9 Structural plan layout of the case study structure: (a) First story and (b) Second to fourth story (unit: mm)

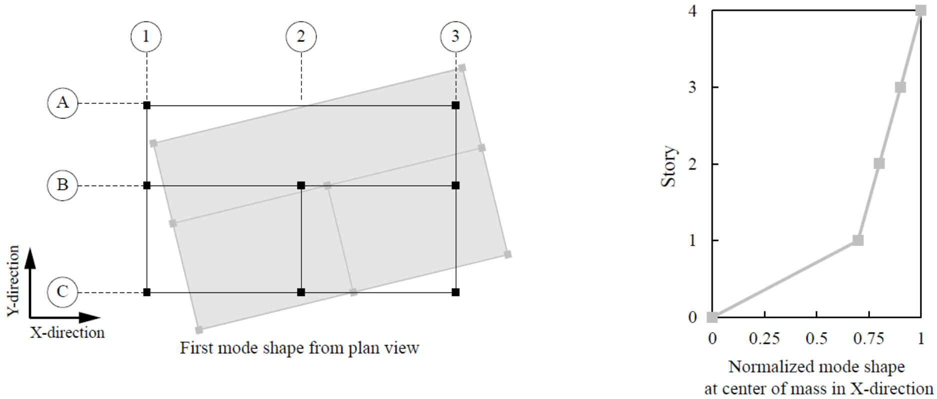

Fig. 10 Fundamental mode shape of the case study structure

The dead and live loads are respectively $600 \ \mathrm{kN/m^2}$ and $300 \ \mathrm{kN/m^2}$. The compressive strength of concrete is 20 MPa and the yield strength of reinforcing bars is 400 MPa. The thickness of the RC walls is 250 mm, which are reinforced with two layers of $\phi12@200$ mm in the transverse and longitudinal directions. The columns have a square section with the dimensions of 400 mm × 400 mm reinforced with $8\phi16$ rebars. The beam sections have the same dimensions as columns with $2\phi14$ rebars at the top and $3\phi14$ rebars at the bottom.

3.2 Analysis model

The analysis model of the case study structure is established in the structural analysis software *OpenSees*. The RC load-bearing walls are modeled using the multilayer shell element. The concrete is subdivided into 2 layers of the cover concrete and 4 core concrete layers. Steel reinforcement layers are embedded layers between the core and the cover concrete layers, and total of 2 horizontal and 2 vertical layers are considered for the transverse and longitudinal rebars at both sides of the wall. The accuracy of this element has been proven in previous studies, which showed that it is capable of capturing the behavior of RC shear walls under large deformations (Lu *et al*. 2015; Shayanfar and Javidan 2017).

The beam members are modeled using the force-based fiber elements with distributed plasticity. The *Concrete01* material with zero tensile strength is utilized to model the concrete, and the *Steel02*, the Giuffré-Menegotto-Pinto material model, is applied for the reinforcing bars. The strain hardening ratio of steel is assumed to be 1% of the initial stiffness. Since the load bearing wall is connected to the beams, beam members are discretized into small elements so that the two nodes of each RC shear wall elements can be connected to the end nodes of a beam element. In that sense, a small number of two integration points along each fiber beam element is enough to capture the accurate behavior. This modeling approach has been compared with experimental tests previously, and is proven to be quite accurate (Amini *et al.* 2018, Shayanfar and Javidan 2017).

On the contrary, column members are modeled using the concentrated plasticity model (Deierlein *et al.* 2010, Javidan and Kim 2019a) to implicitly take into account the shear failure of these members. As the most common failure

Table 1 Details of the earthquake ground motion records used in this research

Record sequence number in PEER Database	Event	Year	Station	Magnitude (M_W)	PGA (g)	R_{rup} (km)	V_{s30} (m/s)
13	Kern County	1952	Pasadena - CIT Athenaeum	7.4	0.06	126	415
14	Kern County	1952	Santa Barbara Courthouse	7.4	0.14	82	515
30	Parkfield	1966	Cholame - Shandon Array #	6.2	0.44	9	299
40	Borrego Mountain	1968	San Onofre - So Cal Edison	6.6	0.05	129	443
141	Tabas, Iran	1978	Kashmar	7.3	0.04	194	280
166	Imperial Valley	1979	Coachella Canal #4	6.5	0.16	50	336
171	Imperial Valley	1979	El Centro - Meloland Geot. Array	6.5	0.38	0.1	265

mechanism in the similar buildings observed in the 2017 Pohang earthquake was shear failure of columns on the first story, it is important to consider this phenomenon in the case study structure. In this regard, columns are modeled using an elastic fiber element and the nonlinearity is concentrated at both ends using two uncoupled nonlinear rotational springs for both the horizontal directions. These springs are modeled using the *Hysteretic* material in *OpenSees* and their backbone curves are defined according to ASCE/SEI 41-13 with a bilinear brittle behavior. In the post-earthquake investigation of damaged structures in the 2017 Pohang earthquake, it was found that the structural details in many soft first story structures were inconsistent with the design code, and as a result the structures failed prematurely before the design strength was reached. This uncertainty effect is not considered in this study and the models are considered to be deterministic; however, such inconsistencies and their effects can be quantified using probabilistic approaches (Javidan *et al*. 2018, Javidan and Kim 2019b).

Lastly, the rigid diaphragm is considered at each story level and Rayleigh damping with 5% of critical damping is assigned to the first two modes of the structure. The loads are distributed to the beams based on the tributary area and the mass is lumped at the mass center of each story.

It is worthwhile to mention that the analysis model as described above consists of 11,135 nodes with six degrees of freedom, 343 nonlinear beam-column elements with fiber sections with 116 fibers each, and 10,224 multilayered shell elements each containing 10 layers. The nonlinear time history analysis of the model is quite costly and it is almost impossible using the conventional interpreters and ordinary personal computers (PC). In this study the computational efficiency is enhanced by the parallel processing technique using the *OpenSeesMP* interpreter. The simulations are carried out using a PC with the Intel® Xeon CPU 12 core processor, and the FE model is divided into 50 parts. The Newmark integrator is utilized and the initial time step is equal to the time step of the ground motion. In the case of convergence problem, the time step is halved adaptively and after twenty successful analysis steps, it is doubled to maintain the computational efficiency.

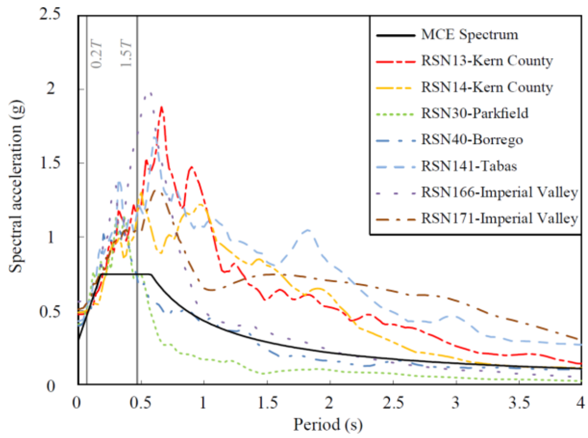

Fig. 11 SRSS spectra of the seven earthquakes scaled to the MCE spectrum

4. Results and discussion

4.1 Seismic performance of the model structure

In order to find out the overall dynamic behavior of the structure, an eigenvalue analysis is carried out first. The fundamental period of the structure is found to be $T = 0.32$ s and the predominant mode shape is shown in Fig. 10, where the largest lateral deformation is observed at the flexible side of the structure in Line C while the stiff side has much smaller displacements due to the core wall located in Line A. The one-way unsymmetrical plan layout of the structure leads to the uneven distribution of plan-wise displacements and torsional behavior. The vertical component of the fundamental mode shape at the center of mass on each story shows that most of the lateral deformation of the structure is concentrated at the first story, and the structure shows the typical behavior of the soft first-story structure. Based on these modal analysis results, it is expected that the load bearing walls on the upper stories remain elastic whereas the first story is subjected to significant damage, especially at the corner columns in the flexible side of the structure.

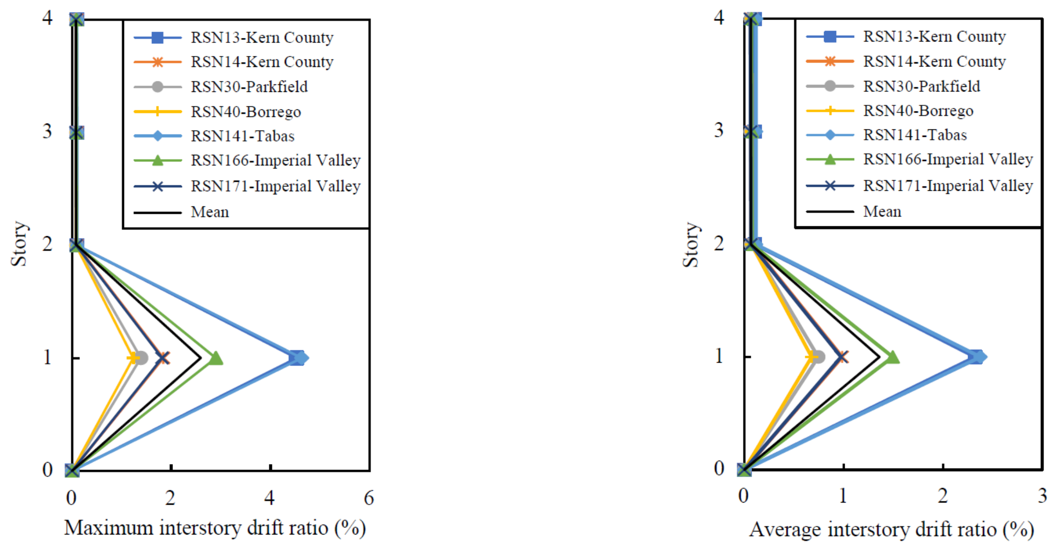

(a) (b)

Fig. 12 Inter-story drift ratios of the case study structure before retrofit: (a) Maximum interstory drift ratio and (b) interstory drift ratio at center of mass

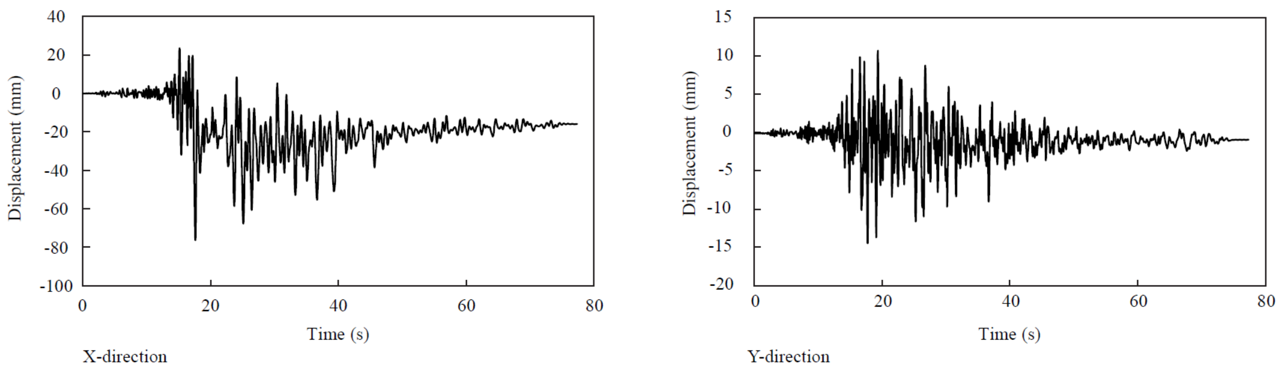

(a) (b)

Fig. 13 Roof displacement time history at the center of mass (RSN13-Kern County earthquake)

Seismic performance of the structure is evaluated using nonlinear time history analysis for earthquake ground motion records applied in both directions. To this end, seven earthquake records containing two horizontal components are chosen from the PEER NGA database (PEER 2014), and are scaled for the maximum considered earthquake (MCE) level of a region in Korea. Details of the earthquakes ground motion records are listed in Table 1, including magnitude, peak ground acceleration (PGA), closest distance to rupture surface R_{rup}, average shear-wave velocity at the top 30 m of soil. The acceleration spectra for the MCE and the seven chosen earthquake records are depicted in Fig. 11. The spectral acceleration for short periods is $S_{MS} = 0.75\ g$ and the corresponding value at the period of 1 s is $S_{M1} = 0.43\ g$. According to ASCE 41-13 (2013), the earthquake ground motion records are scaled in such a way that the average of the SRSS (square root of the sum of square) spectra does not fall below the target spectrum in the range of $0.2T$ and $1.5T$.

Seismic performance of the structure is assessed in terms of the maximum inter-story drift experienced during the seven earthquakes. The results are depicted in Fig. 12 for the corner column where the maximum inter-story drift occurs and also for the center of mass which shows the average inter-story drift. It is observed that the lateral displacement of the structure is concentrated at the soft first story, and the upper stories show negligible relative displacements. Maximum inter-story drift ratios caused by the ground motions range from 1.2% to 4.6% with the mean value of 2.6% while the average inter-story drift ratios at the center of mass are between 0.7% and 2.4% with the mean value of 1.4%. The roof displacement time history of the model structure subjected to the RSN13-Kern County earthquake is depicted in Fig. 13. As expected from the modal analysis, it is observed that the displacements are much larger in the X-direction. There is a residual

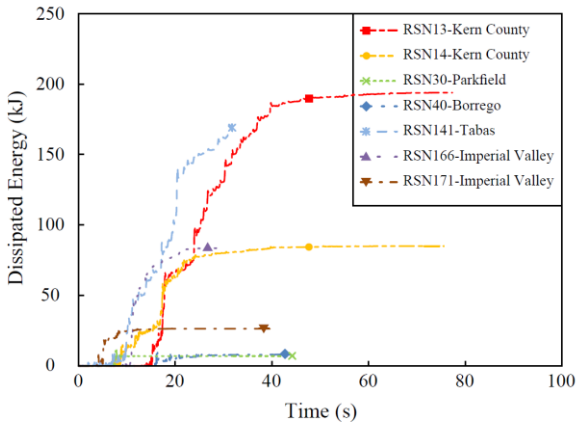

Fig. 14 Dissipated energy in column elements

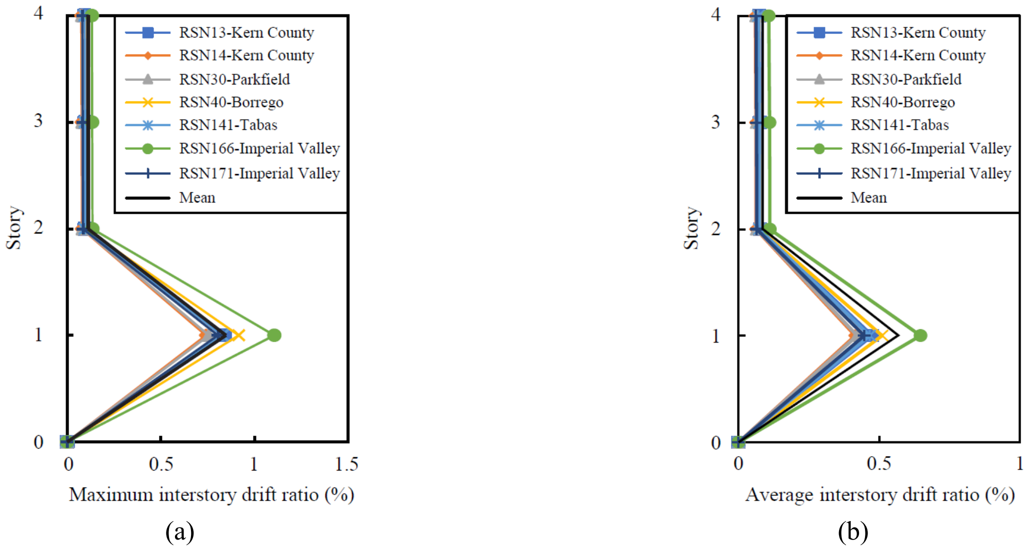

Fig. 15 Inter-story drift ratio of the case study structure after retrofit: (a) Maximum inter-story drift ratio; (b) Inter-story drift ratio at the center of mass

displacement of 16 mm in this direction which is caused by the shear failure of columns with the maximum inter-story drift ratio of 4.5%. Similar responses are observed for the RSN141-Tabas and RSN166-Imperial Valley earthquake records with the maximum interstory drift ratios of 4.6% and 2.9%, respectively.

Since the damage is concentrated at the first story and the RC load bearing walls remain almost elastic, calculation of the energy dissipation for columns can provide a good estimation of the overall damage caused by the earthquakes. Fig. 14 shows the cumulative dissipated energy of columns subjected to the seven earthquake ground motions. It can be seen that the results are consistent with the observed drift ratios. Significant amounts of dissipated energy are observed for the RSN13-Kern County, RSN141-Tabas, and RSN14-Kern County earthquakes, which are respectively 194 kJ, 171 kJ, and 85 kJ. The smallest energy dissipation of 10 kJ is observed when subjected to the RSN40-Borrego earthquake.

4.2 Seismic retrofit of the model structure

The case study structure is retrofitted using the proposed hysteretic damper installed at the flexible side of the structure. According to the eigenvalue analysis and the nonlinear time history analysis results, lateral displacements are larger at this side and the maximum interstory drift occurs at corner columns. Thus, three column dampers designed with the capacity of 100 kN are installed beside the three columns in Line C. The case study structure is reanalyzed under the same earthquake records, and the seismic behavior of the structure is evaluated.

The maximum inter-story drift ratios of the retrofitted structure obtained for the seven earthquakes are plotted in Fig. 15. The maximum inter-story drift ratios are between 0.7% and 1.1% with a mean value of 0.8%, and the average inter-story drift ratios at the center of mass are between 0.4% and 0.6% with a mean value of 0.5%.

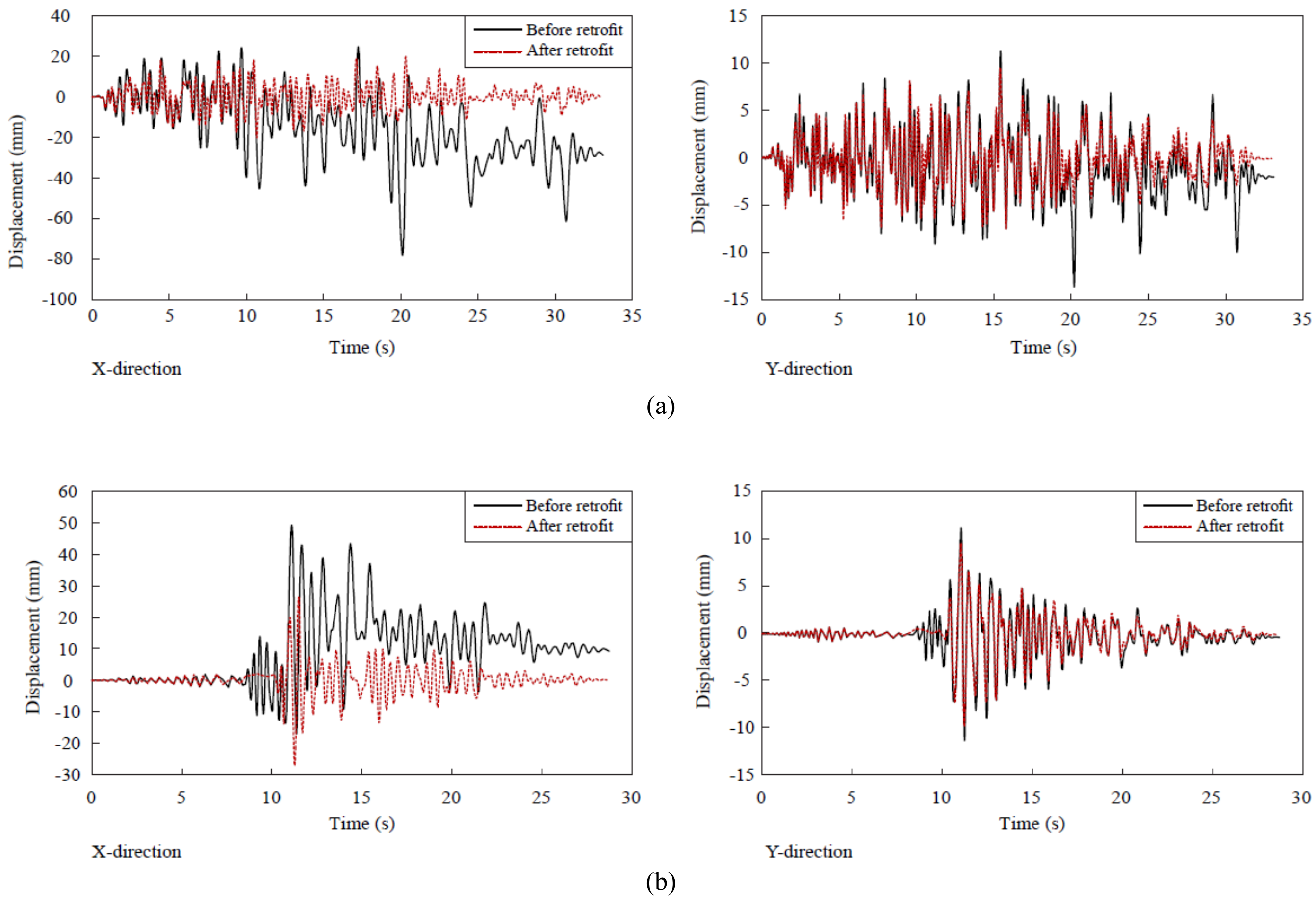

Fig. 16 Roof displacement time histories at the center of mass: (a) RSN141-Tabas and (b) RSN166-Imperial Valley

It is observed that the drift ratios are significantly reduced by implementing the column dampers and the maximum inter-story drift ratios can be limited to the desired level. The roof displacement time histories under the RSN141-Tabas and RSN166-Imperial Valley earthquake ground motions before and after the retrofit are compared in Fig. 16. It can be noticed that the reduction in the residual displacement is considerable, especially in the X-direction. The residual displacements before and after the retrofit in the X-direction are respectively 28.9 mm and 0.5 mm for the RSN141-Tabas earthquake and 9.2 mm and 0.1 mm for the RSN166-Imperial Valley earthquake. This implies that most structural members remain in the elastic range during the earthquakes.

The hysteretic behavior of the dampers under the two abovementioned earthquakes are depicted in Fig. 17. The moment-rotation responses of the nonlinear springs in the upper and lower fuses quantify the energy dissipation in the dampers and the extent of nonlinearity they experience. It can be observed that the dampers show stable hysteretic behavior and dissipate significant seismic energy as expected, resulting in the reduction of the lateral drift. Fig. 18 depicts the cumulative energy dissipated in column members and dampers before and after retrofit. It is interesting to note that the energy dissipation is limited to the dampers, and the column members remain almost elastic.

The fluctuation in energy of the column members is found to be the elastic energy stored as potential energy due to the elastic deformation, and disappears when the member returns back to the initial position. The total energy dissipations are 19 kJ and 16 kJ for the RSN141-Tabas and RSN166-Imperial Valley earthquake ground motions, respectively. The energy dissipations in column members are found to be infinitesimal for all earthquakes, which implies that the structure does not suffer any damage after the considered earthquakes.

It is observed that the damage to the structure can be significantly reduced using a few dampers, and the proposed hysteretic device can be easily designed with required capacity by only adding or reducing steel plates to the fuse section. This makes the damper one of the cheap retrofit techniques. On the other hand, there are also other simple retrofit techniques like steel jacketing (Bahrani et al. 2019). This may be effective in increasing shear resistance of columns, but may not provide enough stiffness and damping capacity required to achieve desired performance levels.

The structure-damper connection needs to act rigidly to guarantee the required energy dissipation in the damper.

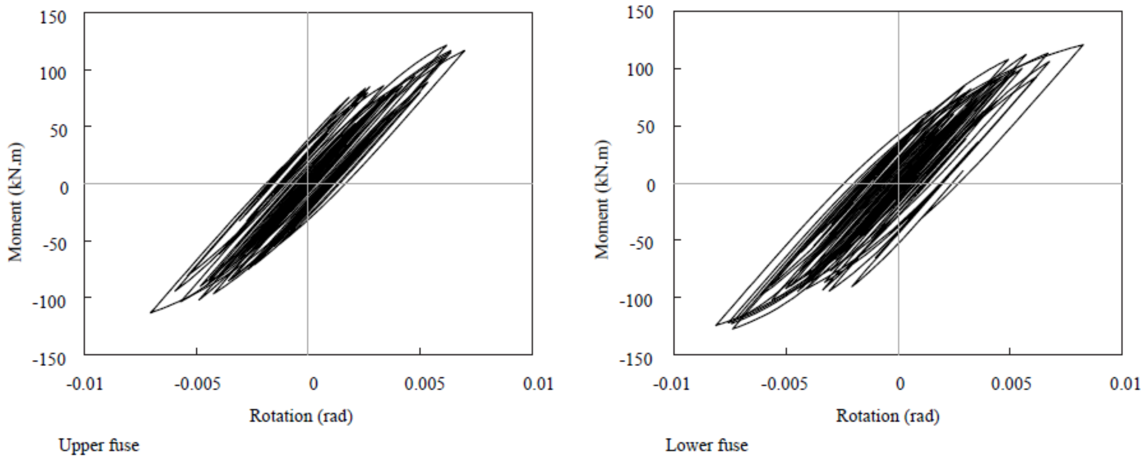

(a)

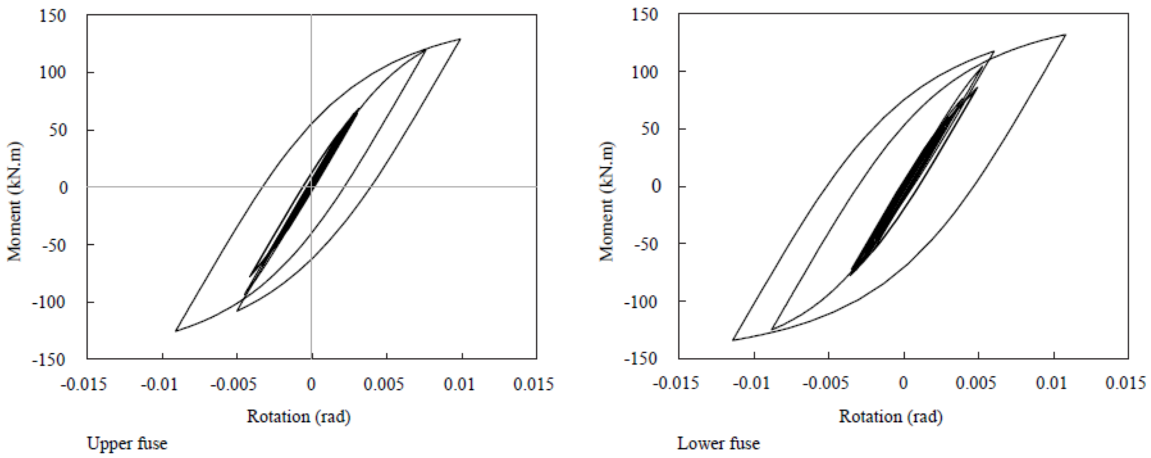

(b)

Fig. 17 Hysteretic behavior of the seismic fuses subjected to the earthquake ground motions: (a) RSN141-Tabas and (b) RSN166-Imperial Valley

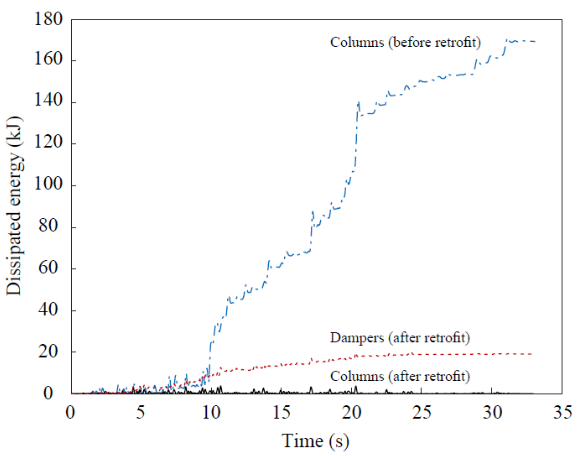

(a)

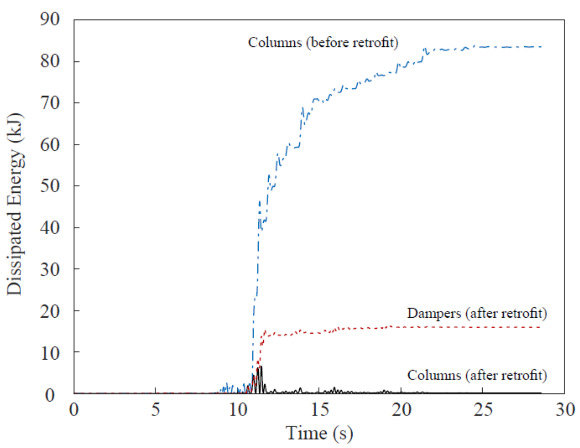

(b)

Fig. 18 Cumulative energy dissipation in columns and dampers before and after retrofit: (a) RSN141-Tabas and (b) RSN166-Imperial Valley

Hence, the damper should be designed within the capacity of the connection including the anchor bolts embedded to the existing structure. Additional steel plates may be required to evenly distribute the moment and shear force induced in the connection, while encasing the beam with steel plate jacket may be needed to protect the beam from the concentrated force. At any rate, experimental study of the developed damper can further improve the practical aspects of the current analytical research.

5. Conclusions

In this study a new hysteretic damper was proposed which consists of one column member and two fuse parts at both ends. The fuse parts are composed of several steel plates with reduced mid-height width which will yield and dissipate seismic energy when subjected to in-plane bending moment. The main advantage of the proposed damper is that it can be placed right beside existing columns and provide the required open space for parking area. Since other types of conventional dampers are usually installed using chevron braces or rigid panels, the proposed device can be very helpful in buildings with architectural limitations. Furthermore, the proposed damper can be easily designed with higher yield capacity due to the in-plane yield of steel plates, while the conventional ADAS and TADAS dampers use out-of-plane bending of steel plates with less amount of energy dissipation.

The nonlinear behavior of the damper including the stiffness and yield force was formulated using elastoplastic analysis, and a procedure was provided to design the damper with a desired capacity. To efficiently implement the proposed damper in seismic retrofit projects, a macromodel was established on the given theoretical premise using the *OpenSees* platform. As an example, a damper was designed and the results from the derived formulas, design procedure, and the macromodel were validated with the detailed FE analysis. It was observed that the provided theoretical formulation could sufficiently describe the behavior of the damper, and the established design procedure could be used to design the dampers with a desired capacity.

The efficiency and applicability of the damper were investigated by retrofitting an RC soft first story structure with one-way asymmetric plan. The seismic performance of the structure was assessed in terms of inter-story drift ratio, residual displacement, and energy dissipation before and after retrofit. Nonlinear dynamic analyses of the structure showed that the proposed damper could effectively protect the case study structure subjected to MCE level earthquake ground motions. Based on the analysis results, it can be expected that the proposed damper can be applied not only to soft-first-story structures but also to other types of structures that have limited space for seismic retrofit.

Acknowledgments

This research was carried out by research funding (task number 19CTAP-C153076-01) of the Ministry of Land, Infrastructure and Transport, Land Transport Technology Promotion Research Project.

References

Agha Beigi, H., Christopoulos, C., Sullivan, T., and Calvi, G.M. (2014), "Gapped-inclined braces for seismic retrofit of soft-story buildings", *J. Struct. Eng*., **140**(11), 4014080. https://doi.org/10.1061/(ASCE)ST.1943-541X.0001006.

Agha Beigi, H., Christopoulos, C., Sullivan, T. and Calvi, M. (2015a), "Seismic response of a case study soft story frame retrofitted using a GIB system", *Earthq. Eng. Struct. D*., **44**(7), 997-1014. https://doi.org/10.1002/eqe.2496.

Agha Beigi, H., Sullivan, T.J., Christopoulos, C., and Calvi, G.M. (2015b), "Factors influencing the repair costs of soft-story RC frame buildings and implications for their seismic retrofit", *Eng. Struct*., **101**, 233-245. https://doi.org/10.1016/j.engstruct.2015.06.045.

Amini, F., Bitaraf, M., Eskandari Nasab, M.S. and Javidan, M.M. (2018), "Impacts of soil-structure interaction on the structural control of nonlinear systems using adaptive control approach", *Eng. Struct*., **157**, 1-13. https://doi.org/10.1016/j.engstruct.2017.11.071.

ANSYS (2019), ANSYS Inc., Canonsburg, PA.

ASCE. (2013), Seismic rehabilitation of existing buildings. ASCE/SEI 41-13, ASCE, Reston, VA.

Bahrani, M.K., Nooralizadeh, A., Usefi, N. and Zargaran, M. (2019), "Seismic evaluation and partial retrofitting of concrete bridge bents with defect details", *Latin Am. J. Solids Struct*., **16**(8), https://doi.org/10.1590/1679-78255158.

Chan, R.W.K. and Albermani, F. (2008), "Experimental study of steel slit damper for passive energy dissipation", *Eng. Struct*., **30**(4), 1058-1066. https://doi.org/10.1016/j.engstruct.2007.07.005.

Dang-Vu, H., Lee, D.H., Shin, J. and Lee, K. (2019), "Influence of shear-axial force interaction on the seismic performance of a piloti building subjected to the 2017 earthquake in Pohang Korea", *Struct. Concrete*, https://doi.org/10.1002/suco.201800291.

Deierlein, G., Reinhorn, A. and Willford, M. (2010), Nonlinear structural analysis for seismic design. National Institute of Standards and Technology (NIST), Gaithersburg, MD.

Javidan, M.M., Kang, H., Isobe, D. and Kim, J. (2018), "Computationally efficient framework for probabilistic collapse analysis of structures under extreme actions", *Eng. Struct*., **172**, 440-452. https://doi.org/10.1016/j.engstruct.2018.06.022.

Javidan, M.M. and Kim, J. (2019a), "Seismic retrofit of soft-first story structures using rotational friction dampers", *J. Struct. Eng*., **145**(12), 4019162. https://doi.org/10.1061/(ASCE)ST.1943-541X.0002433.

Javidan, M.M. and Kim, J. (2019b), "Variance-based global sensitivity analysis for fuzzy random structural systems", *Comput. - Aided Civil Infrastruct. Eng*., **34**(7), 602-615. https://doi.org/10.1111/mice.12436.

Javidan, M.M. and Kim, J. (2020), "Experimental and numerical sensitivity assessment of viscoelasticity for polymer composite materials", *Scientific Reports*, **10**(1), 675-694. https://doi.org/10.1038/s41598-020-57552-3.

Kim, J. and Bang, S. (2002), "Optimum distribution of added VED for mitigation of torsional responses of plan-wise assymetric structures", *Eng. Struct*., **24**(10), 257-269. https://doi.org/10.1016/S0141-0296(02)00046-9.

Kim, J. and Choi, H. (2004), "Behavior and design of structures with buckling-restrained braces", *Eng. Struct*., **26**(6), 693-706. https://doi.org/10.1016/j.engstruct.2003.09.010.

Kim, J. and Jeong, J. (2016), "Seismic retrofit of asymmetric structures using steel plate slit dampers", *J. Constr. Steel Res*., **120**, 232-244. https://doi.org/10.1016/j.jcsr.2016.02.001.

Kim, J. and Kim, S. (2017), "Performance-based seismic design of staggered truss frames with friction dampers", *Thin-Wall. Struct.*, **17**(1), 197-209. https://doi.org/10.1016/j.tws.2016.12.001.

Kim, J., Kim, M. and Nour Eldin, M. (2017), "Optimal distribution of steel plate slit dampers for seismic retrofit of structures", *Steel Compos. Struct.*, **25**(4), 473-484. https://doi.org/10.12989/scs.2017.25.4.473.

Kim, J., Park, J. and Kim, S.D. (2009), "Seismic behavior factors of buckling-restrained braced frames", *Struct. Eng. Mech.*, **33**(3), 261-284. https://doi.org/10.12989/sem.2009.33.3.261.

Lee, J., Kang, H. and Kim, J. (2017), "Seismic performance of steel plate slit-friction hybrid dampers", *J. Constr. Steel Res.*, **136**, 128-139. https://doi.org/10.1016/j.jcsr.2017.05.005.

Lee, J. and Kim, J. (2017), "Development of steel box-shaped slit dampers for seismic retrofit of builidng structures", *Eng. Struct.*, **150**, 934-946. https://doi.org/10.1016/j.engstruct.2017.07.082.

Lu, X., Xie, L., Guan, H., Huang, Y. and Lu, X. (2015), "A shear wall element for nonlinear seismic analysis of super-tall buildings using OpenSees", *Finite Elem. Anal. Des.*, **98**, 14-25. https://doi.org/10.1016/j.finel.2015.01.006.

Mazzoni, S., McKenna, F., Scott, M.H. and Fenves, G.L. (2006), OpenSees command language manual.

Menegotto, M. and Pinto, P.E. (1973), "Method of analysis for cyclically loaded R.C. plane frames including changes in geometry and nonelastic behavior of elements under combined normal force and bending", IABSE Symposium on Resistance and Ultimate Deformability of Structures Acted on by Well-Defined Repeated Loads, Lisbon, 15-22.

Mohammadi, M., Kafi, M.A., Kheyroddin, A., Ronagh, H.R. and Rashidi, M. (2018), "Experimental and numerical investigation of innovative composite buckling-restrained fuse", *Proceedings of the 25th Australasian Conference on Mechanics of Structures and Materials*, Brisbane, 4-7.

Mohammadi, M., Kafi, M.A., Kheyroddin, A. and Ronagh, H.R. (2020), "Performance of innovative composite buckling-restrained fuse for concentrically braced frames under cyclic loading", *Steel Compos. Struct.*, **36**(2), 163-177. http://dx.doi.org/10.12989/scs.2020.36.2.163.

Mualla, I.H. and Belev, B. (2002), "Performance of steel frames with a new friction damper device under earthquake excitation", *Eng. Struct.*, **24**(3), 365-371. https://doi.org/10.1016/S0141-0296(01)00102-X.

Naeem, A. and Kim, J. (2018a), "Seismic retrofit of a framed structure using damped cable systems", *Steel Compos. Struct.*, **29**(3), 287. https://doi.org/10.12989/scs.2018.29.3.287.

Naeem, A. and Kim, J. (2018b), "Seismic performance evaluation of a spring viscous damper cable system", *Eng. Struct.*, **176**, 455-467. https://doi.org/10.1016/j.engstruct.2018.09.055.

Naeem, A. and Kim, J. (2019), "Seismic performance evaluation of a multi-slit damper", *Eng. Struct.*, **189**, 332-346. https://doi.org/10.1016/j.engstruct.2019.03.107.

Nour Eldin, M., Kim, J. and Kim, J. (2018), "Optimal distribution of steel slit-friction hybrid dampers based on life cycle cost", *Steel Compos. Struct.*, **27**(5), 633-646. http://dx.doi.org/10.12989/scs.2018.27.5.633.

Öncü-Davas, S. and Alhan, C. (2019a), "Reliability of semi-active seismic isolation under near-fault earthquakes", *Mech. Syst. Signal Pr.*, **114**, 146-164. https://doi.org/10.1016/j.ymssp.2018.04.045.

Öncü-Davas, S. and Alhan, C. (2019b), "Probabilistic behavior of semi-active isolated buildings under pulse-like earthquakes", *Smart Struct. Syst.*, **23**(3), 227-242. https://doi.org/10.12989/sss.2019.23.3.227.

Park, J., Lee, J. and Kim, J. (2012), "Cyclic test of buckling restrained braces composed of square steel rods and steel tube", *Steel Compos. Struct.*, **13**(5), 423-436. https://doi.org/10.12989/scs.2012.13.5.423.

PEER. (2014), "PEER NGA Database", PEER Ground Motion Database, <https://ngawest2.berkeley.edu/>.

Sahoo, D.R. and Rai, D.C. (2013), "Design and evaluation of seismic strengthening techniques for reinforced concrete frames with soft ground story", *Eng. Struct.*, **56**, 1933-1944. https://doi.org/10.1016/j.engstruct.2013.08.018.

Shayanfar, M.A. and Javidan, M.M. (2017), "Progressive collapse-resisting mechanisms and robustness of RC frame–shear wall structures", *J. Perform. Constr. Fac.*, **31**(5), 4017045. https://doi.org/10.1061/(ASCE)CF.1943-5509.0001012.

Shin, J., Kim, J. and Lee, K. (2014), "Seismic assessment of damaged piloti-type RC building subjected to successive earthquakes", *Earthq. Eng. Struct. D.*, **43**(11), 1603-1619. https://doi.org/10.1002/eqe.2412.

Tsai, C.S., Chen, K.C. and Chen, C.S. (1998), "Seismic resistibility of high-rise buildings with combined velocity-dependent and velocity-independent devices", *Proceedings of the ASME Pressure Vessels and Piping Conference*, San Diego, CA.

Usefi, N., Ronagh, H., Kildashti, K. and Samali, B. (2018), "Macro/micro analysis of cold-formed steel members using Abaqus and OpenSees", *Proceedings of the 13th International Conference on Steel*, Space and Composite Structures, Perth.

Whittaker, A.S., Bertero, V.V., Thompson, C.L. and Alonso, L.J. (1991), "Seismic testing of steel plate energy dissipation devices", *Earthq. Spectra*, **7**(4), 563-604. https://doi.org/10.1193/1.1585644.

Xu, Z.D. (2009), "Horizontal shaking table tests on structures using innovative earthquake mitigation devices", *J. Sound Vib.*, **325**(1-2), 34-48. https://doi.org/10.1016/j.jsv.2009.03.019.

Xu, Z.D., Ge, T. and Liu, J. (2020), "Experimental and theoretical study of high energy dissipation viscoelastic dampers based on acrylate rubber matrix", *J. Eng. Mech. - ASCE*, **146**(6), 04020057. http://doi.org/10.1061/(ASCE)EM.1943-7889.0001802.

Xu, Z.D., Xu, F. and Chen, X. (2016), "Vibration suppression on a platform by using vibration isolation and mitigation devices", *Nonlinear Dynam.*, **83**, 1341-1353. https://doi.org/10.1007/s11071-015-2407-4.

CC